Magnetic reconnection with space and time varying reconnection rates in a compressible plasma

Vladimir S. Semenov
Institute of Physics, State University, St. Petersburg, 198504 Russia

Martin F. Heyn
Institut für Theoretische Physik, Technische Universität Graz, Petersgasse 16, A-8010 Graz, Austria

Ivan B. Ivanov
Petersburg Nuclear Physics Institute, St. Petersburg, 188300 Russia

(Received 6 May 2003; accepted 6 October 2003)

Fast magnetic reconnection of Petschek-type including moving shock waves and discontinuities in a compressible plasma is studied. Magnetic flux tubes of finite size are reconnected by a localized dissipative electric field pulse. This process generates nonlinear perturbations propagating along the initial current surface. The linear wave problem in the outer regions is solved analytically in terms of the reconnection induced sources which move in different directions and with different speeds along the surface. The time-coordinate representation of the solution is given in form of convolution integrals over the reconnection initializing electric field. As an example, reconnection of flux tubes in a sheared magnetic field geometry is analyzed. © *2004 American Institute of Physics.*
[DOI: 10.1063/1.1630055]

I. INTRODUCTION

Magnetic field line reconnection is a fundamental plasma process which is important in numerous cases such as the solar wind interaction with planetary magnetospheres, the energy release in solar flares, transport processes in fusion devices, etc. The ''fast'' reconnection model originally proposed by Petschek[1] considers the global evolution of magnetic flux tubes which have been locally reconnected across an initially magnetically closed current carrying surface. In terms of ideal magnetohydrodynamics (MHD) this is described as a broken tangential discontinuity: a local dissipative electric field[2–4] tangential to the surface leads to a ''breaking'' and ''reconnection'' of magnetic flux tubes. The tangential electric field itself is then transported over the surface by large amplitude MHD waves. This leads to an effective nonlinear release of energy stored within the current surface. More specifically, the surface breaks into a thin boundary layer (BL) which collects plasma from the adjacent reconnected flux tubes and accelerates this plasma to Alfvén speed velocities.

Reconnection in nature is often observed as a time-dependent process of patchy character. To explain these features, the existing analytical solutions for either steady state reconnection in a compressible plasma[5] or time-dependent reconnection in an incompressible plasma[6] have to be extended to cover such an unsteady and patchy behavior. In the present paper, the solution of time varying reconnection in a compressible plasma obtained earlier for plane geometry[7,8] is extended to the more general geometry where skewed fields are reconnected at an X-line of finite length. A magnetic flux tube which has been reconnected across an ideal current surface invalidates the conservation laws for a tangential discontinuity and, in addition, there will appear magnetic flux as well as mass flux normal to the surface. If plasma flows into a surface from both sides, that surface has to broaden into a BL in order to make space for mass conservation. Inside this BL, the plasma is accelerated such that the inertia balances the tangential magnetic stresses of the reconnected flux tubes. The analysis shows that in order to satisfy all conservation laws of ideal MHD across the BL, two shock waves (large amplitude waves) and three discontinuities (large amplitude Alfvén and entropy waves) are necessary. Each reconnected magnetic field line suffers a kink across these large amplitude waves, i.e., current surfaces, and such kinks are known to move with the local de Hoffmann–Teller velocity. Formally this process can be described by the decay of a current surface disturbed by reconnection into a system of large amplitude MHD waves and this process is known as Riemannian problem[5] in the literature.

Recent hybrid simulations of reconnection layers[9] reveal a structure which is similar to the MHD model, but, in addition, show also specific kinetic effects such as ion beams, pressure anisotropy, and dissipation of collisionless character. Kinetic and Hall MHD simulations which have been intensively carried out during the last years,[10–12] emphasizes the importance of Hall effects inside the diffusion region. The central part of this region turned out to extend over a very small scale of the order of inertial electron length. Some evidence of such a diffusion region with Hall effect signatures have been reported recently for a subsolar magnetopause crossing.[13]

In the present study, the shape as well as the spatial localization of the reconnection electric field is assumed *a priori* and from this the plasma flow and magnetic field in the outer, ideal region is computed. In reality, the outer region should be studied together with the nonideal region simultaneously. For some very simple cases attempts have been made to relate the reconnection electric field to dissipation by matching the inner, diffusive solution to the outer,

ideal solution.[4] Simulations of the resistive MHD equations show that the Petschek configuration is observed only for a spatially localized plasma resistivity. In contrast, in the case of a spatially constant plasma resistivity the Sweet–Parker configuration is more likely to apply. Also, kinetic simulations show that the spatial structure of the reconnection electric field is sensitive to the mechanism which breaks magnetic field lines. The present results show how the the parameters in the outer, ideal region depend on the reconnection electric field prescribed along some straight idealized finite reconnection line within a constant, infinitely thin current layer.

For reconnection with $B_n/B_0 \ll 1$ (B_n the magnetic field component normal to the surface), i.e., a sufficiently small dissipative electric field, there are a number of simplifications which allow for analytical progress. First of all, in the case of homogeneous initial conditions above and below the current surface, the de Hoffmann–Teller velocities are constant in lowest order with respect to B_n/B_0. Therefore, the solution of the corresponding Riemannian problem to some extent does not dependent on the actual normal component of the magnetic field which causes the decay. Therefore, a part of the problem can be solved solely in terms of these de Hoffmann–Teller velocities.[5]

The perturbations in form of shocks and discontinuities moving within the BL act as sources for the perturbations in the surrounding medium. The solution in these outer regions is found from the solution of the linearized compressible ideal MHD set of equations supplemented with the appropriate boundary conditions, in particular, total pressure balance as well as mass and magnetic flux conservation at the location of the initial current surface ($z=0$).

In the present paper it is shown how to construct explicitly the outer solution of time varying reconnection of magnetic flux tubes in a compressible plasma. Results for reconnection in skewed magnetic field structures are presented in order to illustrate the method. The solution of the Riemannian problem had been published earlier[5] and some, for the present study necessary, details are collected in the Appendix.

II. THE LINEAR PERTURBATIONS IN THE OUTER REGIONS

Once magnetic flux had been reconnected locally along some idealized line within a current surface, the big scale evolutions of the process can be described in the framework of ideal magnetohydrodynamics (MHD),[14]

$$\frac{\partial \rho}{\partial t} + \mathrm{div}(\rho \mathbf{v}) = 0, \tag{1}$$

$$\frac{\partial (\rho \mathbf{v})}{\partial t} + \mathrm{div}\left[\rho \mathbf{v}\mathbf{v} + p\,\mathbf{I} - \frac{1}{4\pi}\left(\mathbf{B}\mathbf{B} - \frac{B^2}{2}\mathbf{I} \right) \right] = 0, \tag{2}$$

$$\frac{\partial}{\partial t}\left(\frac{1}{2}\rho v^2 + \rho e + \frac{B^2}{8\pi} \right) + \mathrm{div}\left[\rho \mathbf{v}\left(\frac{v^2}{2} + e + \frac{p}{\rho} \right) + \frac{1}{4\pi}\mathbf{B}\times(\mathbf{v}\times\mathbf{B}) \right] = 0, \tag{3}$$

$$\frac{\partial \mathbf{B}}{\partial t} + \mathrm{div}(\mathbf{B}\mathbf{v} - \mathbf{v}\mathbf{B}) = 0. \tag{4}$$

Here ρ is the mass density, $\mathbf{v}$ is the plasma velocity, $\mathbf{B}$ is the magnetic field, p is the isotropic pressure, $e = [1/(\gamma-1)] \times (p/\rho)$ is the internal energy, γ is the polytropic exponent, and $\mathbf{I}$ is the unit diadic. The electric field $\mathbf{E}$ is related to velocity and magnetic field via the ideal Ohm's law, i.e., $\mathbf{E} + (1/c)\,\mathbf{v}\times\mathbf{B} = 0$.

When the ideal MHD equations are linearized with respect to the constant background $\rho^{(0)}$, $\mathbf{v}^{(0)}$, $\mathbf{B}^{(0)}$, all first order MHD quantities can be derived from a displacement vector $\boldsymbol{\xi}(t,\mathbf{x})$,[7]

$$\mathbf{v}^{(1)} = \left(\frac{\partial}{\partial t} + \mathbf{v}^{(0)} \cdot \boldsymbol{\nabla} \right) \boldsymbol{\xi}, \tag{5}$$

$$\mathbf{B}^{(1)} = \mathbf{B}^{(0)} \cdot \boldsymbol{\nabla}\boldsymbol{\xi} - \mathbf{B}^{(0)} \nabla \cdot \boldsymbol{\xi}, \tag{6}$$

$$\rho^{(1)} = -\rho^{(0)} \nabla \cdot \boldsymbol{\xi}, \tag{7}$$

$$p^{(1)} = c_s^2 \rho^{(1)}, \tag{8}$$

$$P^{(1)} = -\rho^{(0)}[u^2 \nabla \cdot \boldsymbol{\xi} + (\mathbf{v}_A \cdot \nabla)\mathbf{v}_A \cdot \boldsymbol{\xi}], \tag{9}$$

where $P^{(1)} = p^{(1)} + \mathbf{B}^{(0)} \cdot \mathbf{B}^{(1)}/(4\pi)$ is the first order total pressure (thermal plus magnetic) and $u^2 = v_A^2 + c_s^2$ is the sum of the squares of zero order values of Alfvén speed v_A and zero order sound speed c_s.

In order to solve the initial-value problem, it is convenient to perform Laplace transformation with respect to time t and Fourier transformation with respect to the coordinates x,y, the plane of the current surface,

$$\frac{\partial}{\partial t} + \mathbf{v}^{(0)} \cdot \nabla \rightarrow p + i\mathbf{v}^{(0)} \cdot \mathbf{k}, \tag{10}$$

$$\nabla \rightarrow (i\mathbf{k}, d/dz), \tag{11}$$

where $p > 0$ and $\mathbf{k} = (k_x, k_y) \in \mathrm{R}^2$. The x and y components of the displacement vector $\hat{\boldsymbol{\xi}}(p,\mathbf{k},z)$ are expressed through the z-component of the displacement vector $\zeta(p,\mathbf{k},z)$, namely,

$$\hat{\boldsymbol{\xi}} = \frac{i}{\Delta}\{p^2[u^2\mathbf{k} - (\mathbf{k}\cdot\mathbf{v}_A)\mathbf{v}_A] + (\mathbf{k}\cdot\mathbf{v}_A)^2 c_s^2 \mathbf{k}\} \frac{d\zeta}{dz}, \tag{12}$$

$$\Delta = p^4 + u^2 k^2 p^2 + (\mathbf{k}\cdot\mathbf{v}_A)^2 c_s^2 k^2. \tag{13}$$

Laplace–Fourier transformation of the z-component of the momentum equation (2) leads to an ordinary differential equation for ζ,

$$\frac{\partial^2 \zeta}{\partial z^2} - q^2(p,\mathbf{k})\zeta = 0, \tag{14}$$

where

$$q^2 = \frac{p^4 + u^2 k^2 p^2 + (\mathbf{k}\cdot\mathbf{v}_A)^2 c_s^2 k^2}{p^2 u^2 + c_s^2 (\mathbf{k}\cdot\mathbf{v}_A)^2}. \tag{15}$$

In the common analysis of surface waves without reconnection, this equation is solved for the upper ζ and the lower $\tilde{\zeta}$ half space separately and the solutions are matched at $z=0$ such that

$$\zeta(p,\mathbf{k},z)|_{z=0}=\tilde{\zeta}(p,\mathbf{k},z)|_{z=0}, \tag{16}$$

$$P^{(1)}(p,\mathbf{k},z)|_{z=0}=\tilde{P}^{(1)}(p,\mathbf{k},z)|_{z=0}, \tag{17}$$

i.e., a unique surface with total pressure balance across it.

In the particular case of reconnection considered in the present analysis, ζ and $\tilde{\zeta}$ have to be different and thus define a thin boundary layer instead of a single perturbed surface. Total pressure balance in first order will still hold across such a BL. The inner structure of the BL is determined by the reconnection electric field in combination with the initial current, i.e., the change in the tangential magnetic field components. The connection between ζ and $\tilde{\zeta}$ is given in the Appendix. The general solution which vanishes at infinity and satisfies first order total pressure balance at $z=0$ is

$$\zeta(p,\mathbf{k},z)=\frac{\tilde{L}e^{-qz}}{L+\tilde{L}}Q(p,\mathbf{k}), \quad z>0, \tag{18}$$

$$\tilde{\zeta}(p,\mathbf{k},z)=-\frac{Le^{\tilde{q}z}}{L+\tilde{L}}Q(p,\mathbf{k}), \quad z<0. \tag{19}$$

Here,

$$L(p,\mathbf{k})=-\rho^{(0)}\frac{p^2+(\mathbf{k}\cdot\mathbf{v}_A)^2}{q(p,\mathbf{k})}, \tag{20}$$

and $\tilde{L}(p,\mathbf{k})$ is of the same form but evaluated for the lower half-space $z<0$. The function $Q(p,\mathbf{k})\equiv\zeta(p,\mathbf{k},0)-\tilde{\zeta}(p,\mathbf{k},0)$ is finite because there are reconnected flux tubes present. The function is obtained from the solution of the boundary layer analysis as shown in the Appendix.

After the solution had been transformed back from frequency-wave number into time-coordinate space, one can construct from $\zeta(t,x,y,z)$ all MHD variables including the horizontal elongation of all discontinuities. In the general case, three integrations are needed. On the other hand, the source term consists of elementary functions of the form

$$\Phi\left(t-\frac{x}{w_x},y-\frac{w_y}{w_x}x\right), \tag{21}$$

and is, therefore, essentially 2D. In that case, the integrations with respect to k_x and k_y can be converted analytically into convolution integrals in time-coordinate space with the help of the 3D generalized Cagniard–deHoop method. This method was originally developed for 2D elastic wave propagation in seismology.[15]

Because the problem is linear, it is sufficient to find the contribution to the displacement vector from one such function, say ζ_Φ. The Laplace–Fourier transform of the shifted Φ function (21) for $x>0$ is

$$\mathcal{L}_t\mathcal{F}_{xy}\left\{\Phi\left(t-\frac{x}{w_x},y-\frac{w_y}{w_x}x\right)\right\}=\frac{w_x\Phi(p,k_y)}{p+i\mathbf{w}\cdot\mathbf{k}}, \quad x>0. \tag{22}$$

The function $\zeta_\Phi(p,x,y,z)$ can be written as a double integral in the form

$$\begin{aligned}\zeta_\Phi(p,x,y,z)&=\frac{1}{(2\pi)^2}\int_{-\infty}^{\infty}dk_x\int_{-\infty}^{\infty}dk_y\frac{\tilde{L}\,e^{-qz+i(k_xx+k_yy)}}{L+\tilde{L}}\frac{w_x\Phi(p,k_y)}{p+i\mathbf{w}\cdot\mathbf{k}}\\&=\frac{2}{(2\pi)^2}\mathrm{Re}\left\{\int_{-\infty}^{\infty}dk_x\int_{0}^{\infty}dk_y\frac{\tilde{L}\,e^{-qz+i(k_xx+k_yy)}}{L+\tilde{L}}\right.\\&\left.\times\frac{w_x\Phi(p,k_y)}{p+i\mathbf{w}\cdot\mathbf{k}}\right\},\end{aligned} \tag{23}$$

where the reality of the function $\zeta_\Phi(p,x,y,z)$, i.e., $\zeta_\Phi(p,-k_x,-k_y,z)=\zeta_\Phi^*(p,k_x,k_y,z)$, had been used to convert the k_y integration. The essential point of the method is to introduce a new set of variables $(k_x,k_y)\rightarrow(s,\alpha)$,

$$k_x=p\,s\,\alpha, \quad \alpha\in(-\infty,\infty), \tag{24}$$

$$k_y=p\,s, \quad s\in(0,\infty). \tag{25}$$

The volume element dk_xdk_y is transformed into $p^2s\,d\alpha ds$ and the integral (23) becomes

$$\begin{aligned}\zeta_\Phi(p,x,y,z)=\frac{2}{(2\pi)^2}\mathrm{Re}\int_{-\infty}^{\infty}d\alpha\int_0^{\infty}ds\,p^2s\\\times\frac{\tilde{L}(s,\alpha)e^{-p[zq(s,\alpha)-is(\alpha x+y)]}}{L(s,\alpha)+\tilde{L}(s,\alpha)}\\\times\frac{1}{p}\frac{w_x\Phi(p,ps)}{[1+is(\alpha w_x+w_y)]},\end{aligned} \tag{26}$$

with

$$\begin{aligned}L(s,\alpha)=-\rho_0(1+s^2\mu^2)\\\times\sqrt{\frac{u^2+c_s^2s^2\mu^2}{1+u^2s^2(1+\alpha^2)+c_s^2(1+\alpha^2)s^4\mu^2}},\end{aligned} \tag{27}$$

$$q^2(s,\alpha)=\frac{1+u^2s^2(1+\alpha^2)+c_s^2(1+\alpha^2)s^4\mu^2}{u^2+c_s^2s^2\mu^2}. \tag{28}$$

Here, $\mu=\alpha v_{Ax}+v_{Ay}$. In the integral (26), the function $\Phi(p,sp)$ can be replaced by $E^*(p,sp)$ using

$$\Phi(p,sp)=\frac{1}{p}\frac{E^*(p,sp)}{B_x/c+isE_z}, \tag{29}$$

which follows directly from (A25) and thus

$$\zeta_\Phi(p,x,y,z)=\frac{1}{2\pi^2}\mathrm{Re}\int_{-\infty}^{\infty}d\alpha\int_0^{\infty}ds\,s \times\frac{\tilde{L}(s,\alpha)e^{-p[zq(s,\alpha)-is(\alpha x+y)]}}{L(s,\alpha)+\tilde{L}(s,\alpha)} \times Q_\Phi(s,\alpha)E^*(p,sp), \tag{30}$$

$$Q_\Phi(s,\alpha)=\frac{w_x}{(B_x/c+isE_z)[1+is(\alpha w_x+w_y)]}. \tag{31}$$

The electric field $E^*(t,y)$ is specified by

$$E^*(t,y)=\frac{1}{\pi}\frac{a}{a^2+y^2}E_1(t), \tag{32}$$

where $a>0$ is constant and $E_1(t)$ is a causal function of time only, i.e., $E_1(t)\equiv 0$ for $t<0$. The general case can be obtained from this form as explained further below. The Fourier transform of the spatial part of the electric field is

$$\mathcal{F}\left\{\frac{1}{\pi}\frac{a}{a^2+y^2}\right\}=e^{-a|k_y|}=e^{-a|sp|}, \tag{33}$$

and one can include $e^{-a|sp|}$ into the exponential factor in the integral (30),

$$\zeta_\Phi(p,x,y,z)=\frac{1}{2\pi^2}\mathrm{Re}\int_{-\infty}^{\infty}d\alpha\int_0^{\infty}ds\,s\frac{\tilde{L}(s,\alpha)}{L(s,\alpha)+\tilde{L}(s,\alpha)} \times Q_\Phi(s,\alpha)E_1(p)e^{-p\tau(s,\alpha)}, \tag{34}$$

where, similar to the 2D case,[7] the function $\tau(s,\alpha)$ is

$$\tau(s,\alpha)=as+zq(s,\alpha)-is(\alpha x+y). \tag{35}$$

At this point one can recognize the advantage of the new variables s and α. The only p-dependent function is now $E_1(p)$ and there is also a p as a coefficient in the exponent. Therefore, if the contour can be analytically deformed in the complex s-plane in such a way that $\tau(s,\alpha)$ becomes real along the whole path of integration, the shift theorem of Laplace transformation $\mathcal{L}^{-1}\{e^{-p\tau}E_1(p)\}=E_1(t-\tau)$ can be applied and immediately gives the time-coordinate representation of the z-component of the displacement vector,

$$\zeta_\Phi(t,x,y,z)=\frac{1}{2\pi^2}\mathrm{Re}\int_{-\infty}^{\infty}d\alpha\int_{\mathcal{C}}ds\,s\frac{\tilde{L}(s,\alpha)}{L(s,\alpha)+\tilde{L}(s,\alpha)} \times Q_\Phi(s,\alpha)E_1(t-\tau(s,\alpha)), \tag{36}$$

with $\mathcal{C}$ such that $\tau(s,\alpha)$ is real for $0\leqslant s\leqslant s_{\max}$ and $s_{\max}(\alpha,t,x,y,z)$, the final point of integration, is defined through causality,

$$\tau(s_{\max},\alpha)\equiv as_{\max}+zq(s_{\max},\alpha)-is_{\max}(\alpha x+y)=t. \tag{37}$$

For $x>0$ and $z>0$, the right half-plane of the complex s plane has to be taken such that there are no contributions to the integral from the arc at infinity when closing the contour to the real s-axis and applying Cauchy's theorem.

If the contributions to the source originating from all discontinuities at $x>0$ and also $x<0$ are taken into account, the time-coordinate representation of the displacement vector becomes

$$\zeta(t,x,y,z)=\frac{1}{2\pi^2}\mathrm{Re}\int_{-\infty}^{\infty}d\alpha\int_{\mathcal{C}}ds\,s\frac{\tilde{L}(s,\alpha)}{L(s,\alpha)+\tilde{L}(s,\alpha)} \times Q_E(s,\alpha)E_1(t-\tau(s,\alpha)), \tag{38}$$

where

$$\begin{aligned}Q_E(s,\alpha)=&\left\{\frac{c}{B_{1x}^+ + is\,cE_{1z}^+}-\frac{c}{B_{0x}+is\,cE_{0z}}\right\}\frac{w_{Ax}^+}{1+is(\alpha w_{Ax}^+ + w_{Ay}^+)}+\left\{\frac{c}{B_{2x}^+ + is\,cE_{2z}^+}-\frac{c}{B_{1x}^+ + is\,cE_{1z}^+}\right\}\frac{w_{Sx}^+}{1+is(\alpha w_{Sx}^+ + w_{Sy}^+)}\\ &+\left\{\frac{c}{\tilde{B}_{1x}^+ + is\,c\tilde{E}_{1z}^+}-\frac{c}{\tilde{B}_{2x}^+ + is\,c\tilde{E}_{2z}^+}\right\}\frac{\tilde{w}_{Sx}^+}{1+is(\alpha\tilde{w}_{Sx}^+ + \tilde{w}_{Sy}^+)}+\left\{\frac{c}{\tilde{B}_{0x}+is\,c\tilde{E}_{0z}}-\frac{c}{\tilde{B}_{1x}^+ + is\,c\tilde{E}_{1z}^+}\right\}\frac{\tilde{w}_{Ax}^+}{1+is(\alpha\tilde{w}_{Ax}^+ + \tilde{w}_{Ay}^+)}\\ &-\left\{\frac{c}{B_{1x}^- + is\,cE_{1z}^-}-\frac{c}{B_{0x}+is\,cE_{0z}}\right\}\frac{w_{Ax}^-}{1+is(\alpha w_{Ax}^- + w_{Ay}^-)}-\left\{\frac{c}{B_{2x}^- + is\,cE_{2z}^-}-\frac{c}{B_{1x}^- + is\,cE_{1z}^-}\right\}\frac{w_{Sx}^-}{1+is(\alpha w_{Sx}^- + w_{Sy}^-)}\\ &-\left\{\frac{c}{\tilde{B}_{1x}^- + is\,c\tilde{E}_{1z}^-}-\frac{c}{\tilde{B}_{2x}^- + is\,c\tilde{E}_{2z}^-}\right\}\frac{\tilde{w}_{Sx}^-}{1+is(\alpha\tilde{w}_{Sx}^- + \tilde{w}_{Sy}^-)}-\left\{\frac{c}{\tilde{B}_{0x}+is\,c\tilde{E}_{0z}}-\frac{c}{\tilde{B}_{1x}^- + is\,c\tilde{E}_{1z}^-}\right\}\frac{\tilde{w}_{Ax}^-}{1+is(\alpha\tilde{w}_{Ax}^- + \tilde{w}_{Ay}^-)}.\end{aligned} \tag{39}$$

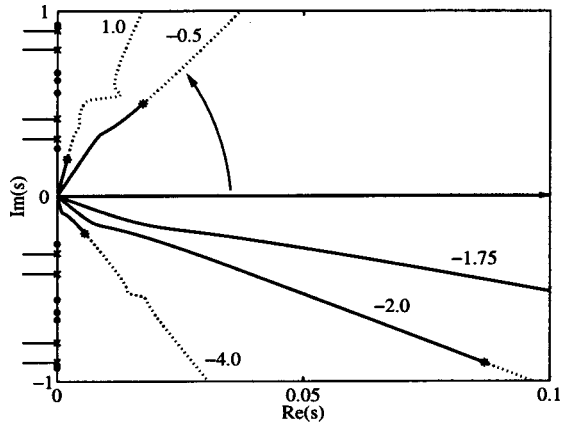

FIG. 1. Sketch of some integration contours $\mathcal{C}$ for several α values in the complex s-plane. Along these contours $\tau(s,\alpha)$ is actually real. On the solid part $0 \leqslant \tau \leqslant t$, on the dashed part $\tau > t$. The endpoints of integration are marked by asterisks. Shown are also branch points (crosses) and poles (dots) on the imaginary axis. Branch cuts are put in the left half plane. The integration along the real axis is converted by applying Cauchy's theorem with an integration in the complex s plane along $\mathcal{C}$.

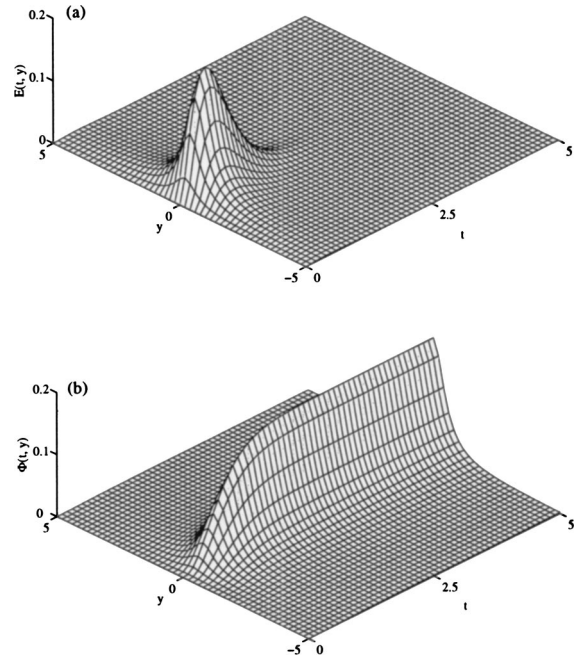

FIG. 2. The time and space variation of the model reconnection electric field $E^*(t,y)$ (top) and the corresponding reconnected flux function $\Phi(t,y)$ (bottom).

Here superscript $(+)$ refers to values for $x>0$ and superscript $(-)$ refers to values for $x<0$ and the details are given in the Appendix.

On the imaginary s-axis there are 12 branch points as well as 16 poles originating from Q_E and 2–4 poles originating from $L+\tilde{L}$ dependent on the initial parameter values. The branch cuts are chosen in the half-space $\mathrm{Re}(s)<0$ (see Fig. 1). Once the endpoint $s_{\max}$ had been determined, the integration contour from $s=0$ to $s=s_{\max}$ in the first quadrant of the complex s-plane can again be suitably deformed if necessary. There are no contribution from $s_{\max}$ to infinity because $E_1(t)\equiv 0$ for $t\leqslant 0$. From the numerical point of view it is more advantageous to perform the integration along a suitable contour where on one hand $\tau(s,\alpha)$ will be complex but on the other hand one can stay away from branch points and singularities, e.g., an arc connecting the origin with $s_{\max}$. For this procedure, the function $E_1(t)$ must have an analytical continuation into the complex plane.

The representation (38) has a simple physical meaning. The integration with respect to s accounts for the contribution from a particular point on the reconnection line marked by α, whereas the integration with respect to α sums up the contributions from all points on the reconnection line. Once the displacement vector (38) has been obtained, all other MHD quantities can be found from (5) to (9).

III. RESULTS AND DISCUSSION

To model a pulse of reconnection one has to specify the dependence of the reconnection rate (32) as a function of time, e.g., as shown in Fig. 2,

$$E^*(t,y)=12t^2e^{-4t}\frac{a}{\pi(a^2+y^2)} \tag{40}$$

with maximal reconnection rate $E^*_{\max}=0.2$. As a function of y, the electric field has a maximum at the origin and then decreases with y. Hence, the constant a in (40) represents an effective length L_X of the reconnection line.

For this type of electric field, the 3D results for the case of purely antiparallel reconnected fields should exactly agree with the 2D results of Ref. 7 in the limit of an infinite long reconnection line. As can be observed in Fig. 3, the 3D separatrix and the distribution of the total pressure really tend to their 2D values and for $a=50$ there is coincide within 0.1% accuracy. The same behavior is observed for the other MHD quantities which are not explicitly shown in the figure. This comparison demonstrates that the 3D method from the previous section gives the correct limit values.

It is interesting that the total pressure distributions corresponding to $a=0.5$ and $a=50$ differ significantly whereas the separatrices do not change much for the whole range $a=0.5-50$. This is due to the fact that the position of the separatrix is mainly defined by the reconnected flux, on the other hand, the distribution of the total pressure depends also on the 3D structure itself.

The 3D effects become really striking when considering reconnection of skewed magnetic fields. The initial parameters of the current surface (tangential discontinuity) and the corresponding solution of the Riemannian problem are presented in Table I. In this table, the magnetic field is normalized to $B_x^{(0)}$, the density to $\rho^{(0)}$, the velocity to $V_A=B_x^{(0)}/\sqrt{4\pi\rho^{(0)}}$, the pressure to $(B_x^{(0)})^2/8\pi$.

Within the time-dependent model of reconnection it is possible to distinguish different phases of the process in terms of a pulsating reconnection rate. During the active phase (the time period when magnetic field lines are reconnected along the X-line, $0<t<2$ in our case) and in the nearest vicinity of the reconnection line time dependent reconnection is very similar to the steady-state Petschek model even for the case of skewed magnetic fields. Thus, for very small periods in a very localized region, one can expect be-

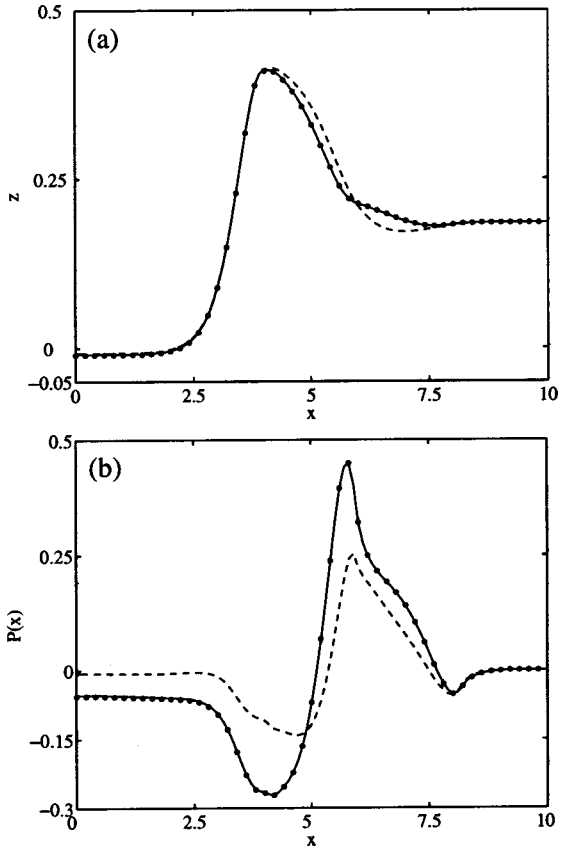

FIG. 3. Comparison of 2D results (points) from Ref. 7 and 3D results from the present paper for the separatrix location (top) and the total pressure distribution (bottom). Solid lines correspond to a long reconnection line ($a=50$) and dashed lines to a short reconnection line ($a=0.5$).

havior similar to classical stationary reconnection. However, most of the time when active reconnection has already stopped, thin boundary layer structures are formed which propagate along the current surface. During this passive phase ($t>2$) the whole MHD structure is essentially three-dimensional and it looks quite different when compared to the stationary Petschek process (Fig. 4).

TABLE I. Plasma parameters in the different regions and the corresponding de Hoffmann–Teller velocities for $x>0$. For $x<0$, the quantities B_x, v_x, and w_x change its sign.

Region	B_x	B_y	v_x	v_y	ρ	p
0 outer	1.0	1.5	0.0	0.0	1.0	4.875
1 AS	−0.701	1.661	1.701	−0.161	1.0	4.875
2 SC	−0.698	1.654	1.697	−0.152	1.003	4.902
$\tilde{2}$ $C\tilde{S}$	−0.698	1.654	1.697	−0.152	1.193	4.902
$\tilde{1}$ $\tilde{S}\tilde{A}$	−0.973	2.303	1.228	0.960	0.7	1.875
$\tilde{0}$ outer	−2.0	1.5	0.0	0.0	0.7	1.875

Wave	w_x	w_y
A	1.0	1.5
S	1.177	1.080
C	1.697	−0.152
$\tilde{S}$	2.039	−0.961
$\tilde{A}$	2.390	−1.793

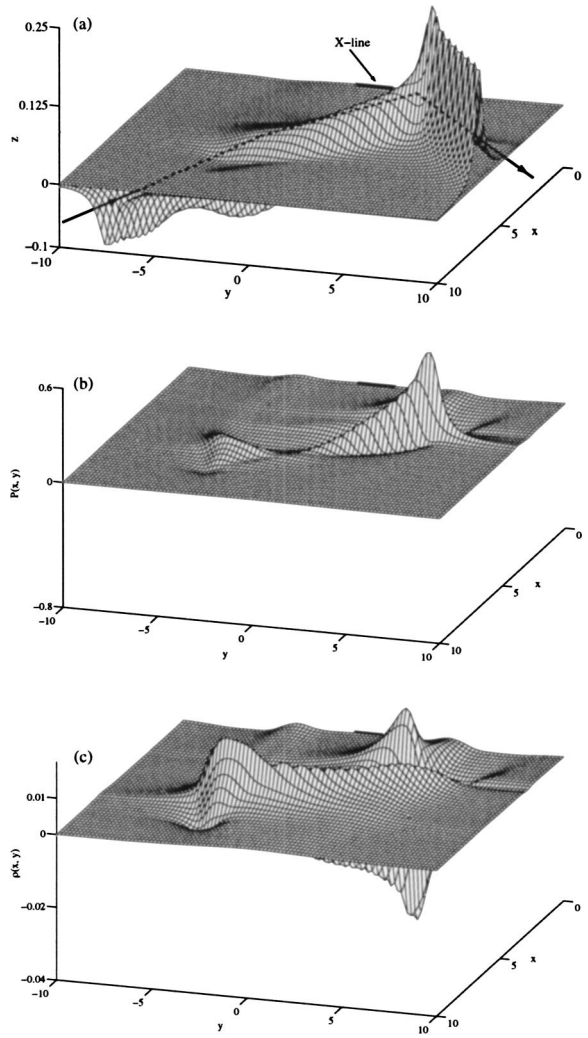

FIG. 4. Reconnection of skewed magnetic fields at time $t=4$. The separatrix surfaces are shown in the top panel. The arrows indicate the direction of the magnetic field above and below the current surface. The corresponding boundary layer structure inside the separatrix surfaces is shown in detail in Fig. 5. The distribution of the total pressure (middle panel) and the plasma density (bottom panel) are shown for $z=0$.

For the case of skewed fields all shocks and discontinuities launched by reconnection move not only with different de Hoffmann–Teller velocities but also they move in different directions. As a result, the BL regions which consist of accelerated and heated plasma are highly elongated with progressively increasing distance between all discontinuities. This can be clearly seen in Fig. 5 where the cross section of the BL region is shown.

Each discontinuity produces disturbances in the outer regions corresponding to the poles of the source term (39). In addition, surface waves connected with the poles of $L+\tilde{L}$ in Eq. (39) must be present. Although the whole structure looks complicated, it is still possible to identify the basic features of skewed field reconnection.

First of all, one has to find the location of the BL region. The Alfvén discontinuities above and below the current surface propagate with different Alfvén velocities $\mathbf{v}_A$, $\tilde{\mathbf{v}}_A$, and in the course of time t, they displace to the positions $\mathbf{v}_A t$, $\tilde{\mathbf{v}}_A t$. Also, the magnetic field between those discontinuities

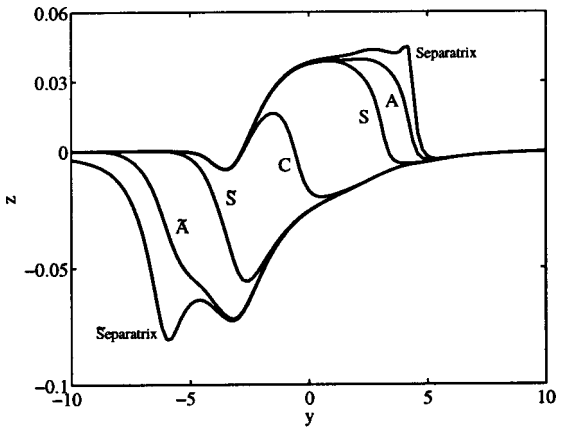

FIG. 5. The evolution of the nonlinear waves initiated by an electric field pulse is shown in a cross section of the boundary layer region corresponding to the direction of the internal magnetic field (central part of dashed line in Fig. 4). Displayed are the separatrix, the Alfvén wave (A), the slow shocks (S), and the contact discontinuity (C).

inside the BL region is directed along the vector $\mathbf{v}_A-\tilde{\mathbf{v}}_A$ (Fig. 4). The cross section of the BL region through its center in the direction of $\mathbf{v}_A-\tilde{\mathbf{v}}_A$ is shown in Fig. 5. The single discontinuities can be observed.

Each discontinuity looks similar to a hill on top of the current surface. The behavior of the MHD perturbations in the outer regions is similar to that found for a moving object such as a wing in pure hydrodynamics. As can be seen from Fig. 4, the density and the total pressure are increased in the front of of moving discontinuities and decreased in the wake.

Any enhancement of the total pressure in the front region must be compensated by a corresponding increase in total pressure in the lower half space. To establish pressure balance, the upper hill is pushed downward which results in the permanent generation of surface waves. This can be seen in Fig. 5.

The scale of the MHD disturbances in the surrounding medium depends on the reconnected flux as well as the size and direction of the reconnected fields. The level of the disturbances in the outer regions strongly depends on the angle between the reconnected fields. In fact, the BL region collects all plasma from the reconnected flux tubes bounded by separatrices. Therefore, the amount of mass, energy and momentum of heated and accelerated plasma inside the BL region linearly increases with time. On the contrary, the reconnected flux during the passive phase is not changed any more. Hence, the more the shocks above and below the current surface separate and the more elongated the BL structure is, the less pronounced are the signatures in the outer regions.

IV. CONCLUSIONS

A new analytical solution of three-dimensional time dependent reconnection in compressible plasma with moving shocks is presented. In this model it is assumed that all dissipative processes responsible for reconnection are localized in an idealized reconnection line of effective finite length and can be taken into account by specifying a time and space varying reconnection rate.

Such an electric field launches a series of large amplitude nonlinear MHD waves which redistribute the initial current and form a structured BL region with accelerated and heated plasma inside. In this way, magnetic energy is effectively converted into kinetic and internal energy of the plasma.

The moving slow shocks and Alfvén discontinuities excite disturbances in the surrounding media. Solutions for a space and time varying reconnection rate are obtained which include coupling of all types of MHD waves (MHD discontinuities and linear slow, fast and Alfvén waves) under the pressure balance condition.

The solution presented above is based on a particular choice of y-dependence of the reconnection rate. This can be easily generalized, i.e., if one writes the electric field with the help of the delta function $\delta(y-y')$ as

$$E^*(t,y)=\int_{-\infty}^{\infty} dy'\ \delta(y-y')E^*(t,y'), \tag{41}$$

the solution can be constructed from the limit $a\to 0$ of the solution above and, therefore, the general solution is

$$\zeta(t,x,y,z)=\frac{1}{2\pi^2}\mathrm{Re}\int_{-\infty}^{\infty} d\alpha \int_{-\infty}^{\infty} dy' \int_C ds\, s \times\frac{\tilde{L}(s,\alpha)}{L(s,\alpha)+\tilde{L}(s,\alpha)}Q_E(s,\alpha) \times E^*(t-\tau(s,\alpha,x,y-y',z),y'), \tag{42}$$

$$\tau(s,\alpha,x,y,z)=zq(s,\alpha)-is(\alpha x+y). \tag{43}$$

One should note that in this representation also the endpoint $s_{\max}$ of the s integration implicitly defined by $\tau(s_{\max},\alpha,x,y-y',z)=t$ depends on y'. The effects of changing the y dependence of the reconnection electric field will be studied in more detail in a future investigation.

The linear part of the problem for the disturbances in the outer regions is equivalent to the evolution of linear perturbations in two half spaces with different anisotropic multimode wave properties coupled by total pressure balance at the interface. Therefore, the presented method can also be applied to analogous surface wave problems in plasma physics or seismology whenever the source is essentially 2D.

ACKNOWLEDGMENTS

V.S.S. and I.B.I. acknowledge financial support from the Technical University Graz and the hospitality of the Institute for Theoretical Physics during a research visit to Graz.

This work has been carried out within the Association EURATOM-ÖAW and with funding from the INTAS-ESA Project No. 99-01277, the Russian Foundation for Basic Research under Grant No. 01-05-64954, and the Austrian Science Fund (FWF) under Contract No. P15956-N08. The con-

tent of the publication is the sole responsibility of its publishers and does not necessarily represent the views of the Commission or its services.

APPENDIX: THE RIEMANNIAN PROBLEM

In this appendix a short summary of the solution of the Riemannian problem is given. A tangential discontinuity is assumed to separate the two half spaces $z>0$ with MHD state vector $\mathbf{U^{(0)}}=(\mathbf{v^{(0)}},\mathbf{B^{(0)}},\rho^{(0)},p^{(0)})$ and $z<0$ with $\tilde{\mathbf{U}}^{(0)}=(\tilde{\mathbf{v}}^{(0)},\tilde{\mathbf{B}}^{(0)},\tilde{\rho}^{(0)},\tilde{p}^{(0)})$. It has been shown earlier[5,7] that the tangential discontinuity disturbed by reconnection decays into a set of large-amplitude Alfvén (A) waves, slow shock (S) or rarefaction (R) waves separated by a contact (C) discontinuity in the center. In the present paper only cases with moderate asymmetry are considered when no rarefaction waves are present. Hence, the set of possible discontinuities will be $ASC\tilde{S}\tilde{A}$.

The solution of the Riemannian problem is defined by the vector

$$\mathbf{h}\equiv \mathrm{sgn}(mB_n)(\tilde{\mathbf{v}}_0-\mathbf{v}_0)+\tilde{\mathbf{v}}_{A0}+\mathbf{v}_{A0}, \tag{A1}$$

where $m\equiv\rho(v_n-D)$ is the mass flux through the discontinuity and D is the speed of the discontinuity. The magnetic field $\mathbf{B}_1$ downstream of the Alfvén discontinuities is parallel to the vector $\mathbf{h}$, i.e.,

$$\mathbf{b}_1=\frac{\mathbf{h}}{\|\mathbf{h}\|}. \tag{A2}$$

The MHD quantities in region AS are

$$\mathbf{B}_1=\mathbf{b}_1B_0, \tag{A3}$$

$$\mathbf{v}_1=\mathbf{v}_0+\mathrm{sgn}(mB_n)(\mathbf{b}_1v_{A0}-\mathbf{v}_{A0}), \tag{A4}$$

$$\rho_1=\rho_0, \tag{A5}$$

$$p_1=p_0, \tag{A6}$$

$$\left(\frac{m}{B_n}\right)_A=\pm\sqrt{\frac{\rho}{4\pi}}, \tag{A7}$$

$$\mathbf{w}_A\equiv\mathbf{v}-\frac{1}{\rho}\left(\frac{m}{B_n}\right)_A\mathbf{B}. \tag{A8}$$

Here $\mathbf{w}_A$ is the de Hoffmann–Teller velocity of the Alfvén discontinuity. Similar formulas are valid for the region $\tilde{A}\tilde{S}$.

To find the MHD quantities in the region $SC\tilde{S}$ it is convenient to use as a key parameter the change in magnetic strength across the slow shock $\eta=B_2/B_0$, and $\tilde{\eta}=\tilde{B}_2/\tilde{B}_0$. Since the magnetic field is continuous across the contact discontinuity, one can write $\eta B_0=\tilde{\eta}\tilde{B}_0$. Then, the parameter η can be calculated from

$$\|\mathbf{h}\|=v_{A0}G(\eta)+\tilde{v}_{A0}G(\tilde{\eta}), \tag{A9}$$

where the function G is defined as

$$G(\eta)=1-\sqrt{(1-\eta)\left(1-\left[\frac{1-\eta^2}{2\beta+(\gamma-1)(1-\eta)}\right]\eta\right)}, \tag{A10}$$

with $\beta=c_s^2/v_{A0}^2$ and γ the polytropic index. Note that across the slow shock the magnetic strength decreases, hence $\eta<1$ and $\tilde{\eta}<1$. After η had been found, the MHD values downstream of the slow shock are

$$\mathbf{B_2}=\mathbf{b_1}\eta B_0, \tag{A11}$$

$$\mathbf{v_2}=\mathbf{v_0}-\mathrm{sgn}(mB_n)[\mathbf{v}_{A0}-\mathbf{b_1}v_{A0}G(\eta)], \tag{A12}$$

$$\frac{\rho_2}{\rho_0}=1+\frac{1-\eta^2}{2\beta+(\gamma-1)(1-\eta)}, \tag{A13}$$

$$p_2=p_0+\frac{B_0^2}{8\pi}(1-\eta^2), \tag{A14}$$

$$\left(\frac{m}{B_n}\right)_S=\pm\frac{1}{\sqrt{4\pi}}\sqrt{\frac{\eta-1}{\dfrac{\eta}{\rho_2}-\dfrac{1}{\rho_1}}}, \tag{A15}$$

$$\mathbf{w}_S\equiv\mathbf{v}-\frac{1}{\rho}\left(\frac{m}{B_n}\right)_S\mathbf{B}. \tag{A16}$$

The local horizontal elongation of the shocks will be of first order in B_n/B_0, say,

$$z=f(t,x,y), \tag{A17}$$

and, therefore, normal vector $\mathbf{n}$ and shock speed D are

$$\mathbf{n}=(-f_x,-f_y,1),\quad D=f_t, \tag{A18}$$

since $\sqrt{1+f_x^2+f_y^2}\approx 1$ in lowest order. Therefore, mass flux and normal magnetic field are

$$m=\rho(v_n-D)=\rho\left(-\mathbf{v}^0\cdot\nabla f+\frac{\partial\zeta}{\partial t}+\mathbf{v}^0\cdot\nabla\zeta-\frac{\partial f}{\partial t}\right), \tag{A19}$$

$$B_n=(-\mathbf{B}^0\cdot\nabla f+\mathbf{B}^0\cdot\nabla\zeta). \tag{A20}$$

Then the Walén relation at the Alfvén discontinuity (A8) and at the slow shock (A16) lead to the equation

$$\left(\frac{\partial}{\partial t}+\mathbf{w}^{(0)}\cdot\nabla\right)(f-\zeta)=0, \tag{A21}$$

with a solution

$$f(t,x,y)=\zeta(t,x,y)+\Phi\left(t-\frac{x}{w_x^{(0)}},y-\frac{w_y^{(0)}}{w_x^{(0)}}x\right), \tag{A22}$$

where the velocity $\mathbf{w}$ had been defined above. The y-component of the electric field within any discontinuity in its rest frame is

$$E^*(t,x,y) := \frac{1}{c}((\mathbf{v}-D\mathbf{n})\times\mathbf{B})\cdot(\mathbf{n}\times\mathbf{e}_x)$$
$$= \frac{B_x^{(0)}}{c}(v_n - D) - \frac{B_n}{c}(v_x^{(0)} - Dn_x)$$
$$\approx \frac{B_x^{(0)}}{c}(v_n - D) - \frac{B_n}{c}v_x^{(0)}$$
$$= \frac{B_x^{(0)}}{c}\frac{\partial\Phi}{\partial t}\left(t - \frac{x}{w_x^{(0)}}, y - \frac{w_y^{(0)}}{w_x^{(0)}}x\right)$$
$$+ E_z^{(0)}\frac{\partial\Phi}{\partial y}\left(t - \frac{x}{w_x^{(0)}}, y - \frac{w_y^{(0)}}{w_x^{(0)}}x\right), \quad \text{(A23)}$$

if the expressions (A19)–(A20) for B_n and $v_n - D$ are used. Here,

$$E_z^{(0)} = \frac{1}{c}(v_y^{(0)}B_x^{(0)} - v_x^{(0)}B_y^{(0)}). \quad \text{(A24)}$$

All discontinuities cross the reconnection line at $x=0$ and, therefore, the function $\Phi(t,y)$ is defined through the electric field along the reconnection line in its rest frame by evaluating (A23) at $x=0$,

$$\frac{B_x^{(0)}}{c}\frac{\partial\Phi}{\partial t}(t,y) + E_z^{(0)}\frac{\partial\Phi}{\partial y}(t,y) = E^*(t,y). \quad \text{(A25)}$$

The solution of (A25) is

$$\Phi(t,y) = \frac{c}{B_x^{(0)}}\int_0^t d\tau\, E^*\left[\tau, y - \frac{cE_z^{(0)}}{B_x^{(0)}}(t-\tau)\right]. \quad \text{(A26)}$$

The function $f(t,x,y)$ describes the shape of the discontinuities and therefore it must be the same if (A22) is evaluated at the different sides of the discontinuities. These conditions give the connections between the z-components of the displacement vector ζ in the different regions

$$\zeta_0 + \Phi_0(\mathbf{w}_A^{(0)}) = \zeta_1 + \Phi_1(\mathbf{w}_A^{(0)}), \quad (A), \quad \text{(A27)}$$

$$\zeta_1 + \Phi_1(\mathbf{w}_S^{(0)}) = \zeta_2 + \Phi_2(\mathbf{w}_S^{(0)}), \quad (S), \quad \text{(A28)}$$

$$\zeta_2 = \tilde{\zeta}_2, \quad (C), \quad \text{(A29)}$$

$$\tilde{\zeta}_2 + \tilde{\Phi}_2(\tilde{\mathbf{w}}_S^{(0)}) = \tilde{\zeta}_1 + \tilde{\Phi}_1(\tilde{\mathbf{w}}_S^{(0)}), \quad (\tilde{S}), \quad \text{(A30)}$$

$$\tilde{\zeta}_1 + \tilde{\Phi}_1(\tilde{\mathbf{w}}_A^{(0)}) = \tilde{\zeta}_0 + \tilde{\Phi}_0(\tilde{\mathbf{w}}_A^{(0)}), \quad (\tilde{A}), \quad \text{(A31)}$$

with

$$\Phi_i(\mathbf{w}_j^{(0)}) \equiv \Phi_i\left(t - \frac{x}{w_{jx}^{(0)}}, y - \frac{w_{jy}^{(0)}}{w_{jx}^{(0)}}x\right), \quad \text{(A32)}$$

evaluated with (A26) in region i, and $j = A, S, \tilde{A}$, or $\tilde{S}$. Therefore, the source term $Q(t,x,y) = \zeta_0(t,x,y) - \tilde{\zeta}_0(t,x,y)$ in (19) is

$$Q(t,x,y) = \Phi_1(\mathbf{w}_A^{(0)}) - \Phi_0(\mathbf{w}_A^{(0)}) + \Phi_2(\mathbf{w}_S^{(0)}) - \Phi_1(\mathbf{w}_S^{(0)})$$
$$+ \tilde{\Phi}_1(\tilde{\mathbf{w}}_S^{(0)}) - \tilde{\Phi}_2(\tilde{\mathbf{w}}_S^{(0)}) + \tilde{\Phi}_0(\tilde{\mathbf{w}}_A^{(0)}) - \tilde{\Phi}_1(\tilde{\mathbf{w}}_A^{(0)}) \quad \text{(A33)}$$

which follows from the summation of (A27)–(A31). The de Hoffmann–Teller velocities $\mathbf{w}^{(0)}$ are different for the $x>0$ and $x<0$ half-spaces because the waves propagate in opposite direction away from the reconnection line. Hence, the Laplace–Fourier transform has to be done separately for $x>0$ and $x<0$ which doubles the number of terms in (A33). Note, that a minus sign has to be taken in the Laplace–Fourier transform of the shifted Φ function (22) for $x<0$,

$$\mathcal{L}_t\mathcal{F}_{xy}\left\{\Phi\left(t - \frac{x}{w_x}, y - \frac{w_y}{w_x}x\right)\right\} = -\frac{w_x\Phi(p,k_y)}{p + i\mathbf{w}\cdot\mathbf{k}}, \quad x<0. \quad \text{(A34)}$$

If each of the $\Phi(p,k_y)$ functions is replaced by $E^*(p,k_y)$ using the Laplace–Fourier transform of Eq. (A25), the representation (39) for $Q_E(s,\alpha)$ is found.

[1] H. E. Petschek, in *AAS-NASA Symposium of the Physics of Solar Flares, NASA-SP 50*, edited by W. N. Hess (National Aeronautics and Space Administration, Washington, D.C., 1964), pp. 425–439.
[2] M. Scholer, J. Geophys. Res. **94**, 8805 (1989).
[3] M. Ugai, Phys. Plasmas **2**, 388 (1995).
[4] N. V. Erkaev, V. S. Semenov, and F. Jamitzky, Phys. Rev. Lett. **84**, 1455 (2000).
[5] M. F. Heyn, H. K. Biernat, R. P. Rijnbeek, and V. S. Semenov, J. Plasma Phys. **40**, 235 (1988).
[6] V. S. Semenov, V. V. Lebedeva, H. K. Biernat, M. F. Heyn, R. P. Rijnbeek, and C. J. Farrugia, J. Geophys. Res. **100**, 21779 (1995).
[7] M. F. Heyn and V. S. Semenov, Phys. Plasmas **3**, 2725 (1996).
[8] V. S. Semenov, O. A. Drobysh, and M. F. Heyn, J. Geophys. Res. **103**, 11863 (1998).
[9] M. Cremer and M. Scholer, J. Geophys. Res. **105**, 27621 (2000).
[10] J. Birn, J. F. Drake, M. A. Shay *et al.*, J. Geophys. Res. **106**, 3715 (2001).
[11] P. L. Pritchett, J. Geophys. Res. **106**, 25961 (2001).
[12] J. C. Dorelli and J. Birn, J. Geophys. Res. **108**, 1133 (2003).
[13] F. S. Mozer, S. D. Bale, and T. D. Phan, Phys. Rev. Lett. **89**, 015002 (2002).
[14] A. I. Akhiezer, I. A. Akhiezer, R. V. Polovin, A. G. Sitenko, and K. N. Stepanov, *Plasma Electrodynamics* (Pergamon, Oxford, 1975).
[15] T. Rikitake, R. Sato, and Y. Hagiwara, *Applied Mathematics for Earth Scientists* (Terra Scientific, Tokyo, 1987).